Liquid Film Cooling: Open-Literature Review, Modeling and Efforts Towards Validation

Federico Giambelli[*], *Riccardo Bisin*[*], *Enrico Bragalli*[*] *and Christian Paravan*[*†]
[*]*Politecnico di Milano, Department of Aerospace Sciences and Technologies*
34 Via La Masa, Milan, I-20156
federico.giambelli@polimi.it · riccardo.bisin@polimi.it · enrico.bragalli@mail.polimi.it · christian.paravan@polimi.it
[†]Corresponding author

Abstract

Liquid film cooling is one of the possible solutions for the thermal control of liquid rocket engine thrust chambers. An open literature review of models for the determination of liquid film cooling length is completed. Moving forward, an extended version of one of the previous models is developed, including effects that are generally neglected, such as the entrainment. With the resulting model, the evolution of a 1D thin liquid layer can be tracked along the longitudinal engine axis, under the influence of a high-enthalpy core stream. Open-literature data are used for the validation of the extended model.

1. Introduction

Liquid Rocket Engines (LREs) embody a preeminent role in thermo-chemical propulsion and are largely employed in multiple applications: from space access to in-space maneuvering. Depending on the type of mission, LREs may feature different thrust levels and firing times. The basic principle of functioning relies on the conversion of enthalpy, generated from combustion, into kinetic energy via a gas-dynamic nozzle. In this groundwork, large heat fluxes are generated in the thrust chamber (with peak values that are reached at the nozzle throat). Consequently, an efficient cooling method is requested during the entire operating lifetime of a liquid propellant engine.[13]

Among all the possible engine cooling strategies, film cooling (FC) is one of the possible solutions, being first studied in the 1950s,[4,15,18] and practically applied on board the Saturn V launcher.

The film cooling working principle relies upon the interposition of a thin coolant layer (i.e., fuel) to protect the chamber walls beneath. Transpiration and slow diffusion of the film into the core stream are exploited, persisting in the form of a protective layer.[28] Therefore, in film-cooled systems, the prediction of either (i) the length until the film persists, and (ii) the temperature profile due to the mainstream gas are assessed.

In film-cooled thrust chambers, both gaseous (GFC) and liquid film cooling (LFC) may be exploited for thermal control. In the former, gaseous coolant is introduced in the thrust chambers via dedicated injectors, exploiting slow diffusion, and reducing the heat flux reaching the walls beneath.[27] The curtailment of the heat flux passes also through the mixing process with the core stream boundary layer, for which a similar velocity profile and uniform temperature are retrieved, obeying the classical laws.[8,28] In liquid film cooling, the coolant is injected in liquid state, typically fuel is selected to limit chemical oxidation. The thin liquid layer absorbs heat from the mainstream gas, via convection and radiation. The coolant temperature increases, reaching the saturation point, above which, vaporization starts. As a consequence, the liquid film cooling is more effective than its gaseous counterpart, due to the transpiration mechanism and aggregation state transition. For this effect, LFC is more attractive for liquid rocket propulsion.

Advantages of FC arise in the lower wall temperatures, lower overall pressure drops, and lower power-plant weight than regenerative cooling.[24] Recently, efforts on LFC have been reviewed by Shine et al.[28] who developed a simple analytical model for the prediction of Liquid Film Cooled-Length (FCL).[27] This work followed the early research of Grissom[9] in this field. Wide and detailed numerical and experimental campaigns for the understanding of FC-related phenomena have been performed by Kircheberger et al.[16,17]

In the present work primary attention is given to liquid film cooling. The underlying physical mechanism is outlined, focusing on the most widely employed pre-existing models. Once this part is concluded, a new approach is developed on the basis of Grissom's[9] and Shine's[27] works, with the aim of enhancing the accuracy of existing modeling strategies, introducing some aspects that are in general neglected. To fill this modeling and accuracy gap, the film hydrodynamic stability is deeply studied, assessing the amount of coolant mass that is lost due to the core stream shearing action by entrainment mass transfer.[7,9,14,27] In most of the models, this aspect is briefly touched or directly discarded due

to the complex nature of the phenomenon. In the present work, attention is paid to modeling this aspect, which is of paramount importance for accurate predictions of the liquid film-cooled length. The document is closed with a wide model validation procedure replicating multiple experimental campaigns.[7, 15, 16, 18, 24]

2. Open-Literature Models Review

In this section (i) the fundamental physical principles behind liquid film cooling are presented, and (ii) open-literature models for the analysis of the liquid layer length are reviewed. Results from the models are contrasted considering existing experimental data sets. The relevant governing equations concerning the basic liquid film cooling mechanism are mass and energy balance. Regarding the pre-existing models, the one from Grissom[9] is deeply investigated, becoming the starting point for the development of the model proposed by the authors of this paper. In existing open-literature models, relevant quantities, such as coolant temperature and flow rate, are tracked along the engine longitudinal axis when subjected to a high enthalpy core stream.

2.1 Liquid Film Cooling Physical Principle

Liquid film cooling features the injection of coolant in liquid form, where, potentially, both fuel and oxidizer can be exploited. Nonetheless, fuel is desired due to the null oxidative chemical action, which may be aggressive for the metal chamber walls. As for GFC, the liquid coolant is introduced in the thrust chamber via dedicated injectors, covering the internal walls. The shielding process passes through the absorption of the enthalpy stream, via radiation and convection,[9] increasing the coolant temperature up to the saturation point. At this stage, the evaporation is triggered, engendering the following effects: (i) the coolant absorbs the latent heat of gasification, (ii) the mass blowing from the coolant reduces the convection mechanism via the blockage effect,[9, 27] and (iii) the vaporized mass acts as a buffer layer, still protecting the thrust chamber walls. This peculiar process allows for the slow diffusion of the vaporized coolant inside the propellant core stream, hence ensuring proper protection. In this framework, a key parameter for the evaluation of the liquid film cooling effectiveness is the length the liquid coolant endures for, the FCL.
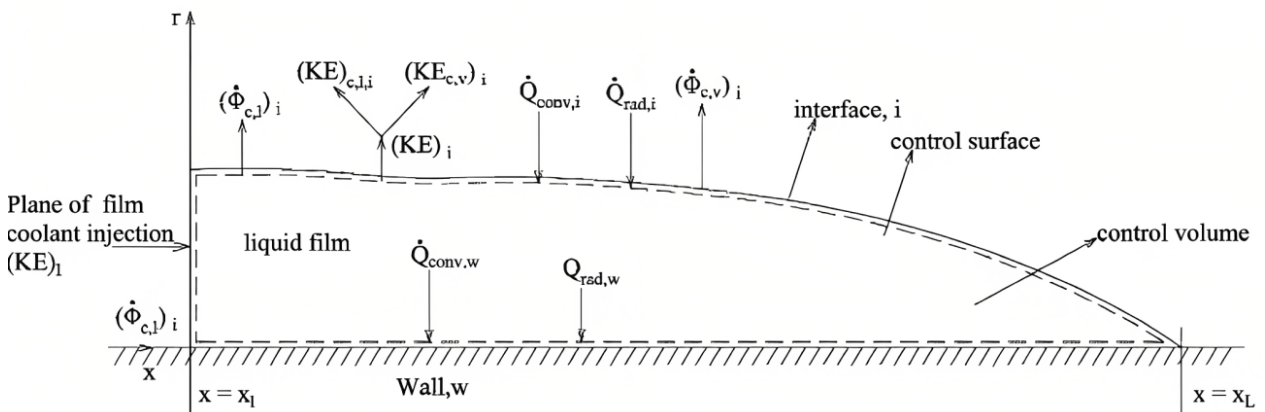

Figure 1: Liquid film cooling: energy balance on the control volume and layer thinning due to the coolant vaporization.[27]

As presented in Figure 1, the liquid film cooling analysis is driven by (i) mass, and (ii) energy conservation equations inside the control volume. Through the energy equation, the coolant temperature variation is assessed. Concerning the mass, it may be lost as an effect of two concurring mechanisms: entrainment of liquid droplets and vaporization. Entrainment is a peculiar mass transfer originating from core flow shearing action exerted onto the thin liquid layer. The shear stress tends to make the liquid layer unstable, generating roll waves on its free surface, possibly causing droplets detachment, when inertia forces overcome the surface tension ones.[7, 14] This phenomenon may occur prior to, and after the saturation is reached. Beside mass losses, entrainment acts on the increased surface roughness, enhancing the convective heat transfer, and impacting the liquid mass flow rate decrease.[27]

For his fact, the model developed in the next sections aims at filling this gap by borrowing from the HRE background, trying to enhance the accuracy of the FCL prediction.

2.2 Liquid Film Cooling Models

In this section, open-literature models for the analysis of LFC are presented and reviewed. Discussion follows a chronological order. The reviewed models are (i) the one by Stechman and co-workers,[29] (ii) NASA SP-8124,[6] (iii) the model by Grissom,[9] and (iv) the one proposed by Shine.[27]

Stechman developed a model for film cooling effectiveness prediction in small liquid rocket engines,[29] exploiting global balances of mass and energy at the film surface. Starting from the energy equation, the heat flux reaching the film is evaluated as follows:

$$\frac{\dot{q}}{A} = h_g \left(T_{Eff} - T_w \right) \tag{1}$$

In Eq. 1 an effective gas temperature in the presence of non-adiabatic walls is considered: T_{Eff}. In the approach proposed by Ref.,[29] the analysis is focused on the wall temperature (T_w). The value of this parameter is determined based on the coupling between the propellant stream and the coolant. The FCL is here defined as:

$$L_c = \frac{\zeta W_c c_c \left(T_{Vap} - T_{Inj} \right)}{P_e h_g \left(T_r - T_{Sat} \right)} + \frac{\zeta W_c \gamma}{P_e h_g \left(T_r - T_{Sat} \right)} \tag{2}$$

Looking at Eq. 2, the total liquid length is the sum of two different contributions: the first one (at the right-hand side) provides the distance (from the coolant injection point) the saturation temperature is reached at. The second term estimates the distance for which temperature is constant, at the saturation level, and the vaporization process is in-proceeding. In both terms, the stability of the film is expressed via the ζ parameter, bounded between 0 and 1, a function of the coolant Reynolds number (Re_c) defined hereby:

$$Re_c = \frac{W_c}{\pi D_{CC} \mu_c} \tag{3}$$

The effective gas temperature is now evaluated downstream of the coolant injector, in the gaseous coolant region, as presented below:

$$\frac{T_r - T_{Eff}}{T_r - T_{Sat}} = \exp \left(-\frac{h_g A}{\Phi c_c W_c} \right) \tag{4a}$$

$$\frac{1}{\Phi} = \left(\frac{\delta_c u_g}{u_c} \right)^{1/8} f(\beta) \qquad \beta = \frac{u_g}{u_c} \tag{4b}$$

$$f(\beta) = (1/\beta)^{-1.5 \left(\beta^{-1} - 1 \right)}, \qquad \beta \leq 1 \tag{4c}$$

$$f(\beta) = 1 + 0.4 \tanh (\beta - 1), \qquad \beta > 1 \tag{4d}$$

The above relations are retrieved from the results of Hatch and Papell,[10] assuming that: i) the coolant does not exhibit mixing nor chemical reaction with the core stream flow, ii) the coolant temperature does not change as rapidly as the coolant moves downstream, iii) the gradients across the thin coolant film are small, and iv) no conduction heat transfer occurs inside the chamber walls.

At this stage, the missing parameters to be defined are the convection heat transfer coefficients: at the gas-coolant and coolant-wall sides. Starting from the former, the turbulent gas-coolant convection heat transfer coefficient is evaluated with the implementation of the Bartz equation,[1] including minor modifications,[29] allowing for variable coolant thermo-physical properties:

$$h_g = 0.026 \frac{\mu_g^{0.2}}{D_{cc}^{*0.2} Pr_g^{0.667}} \left(\frac{W}{A^*} \right)^{0.9} \left(\frac{A^*}{A} \right)^{0.9} \left(\frac{H_r - H_w}{T_r - T_w} \right) n \tag{5}$$

Moving to the coolant-wall side, the heat transfer coefficient is evaluated assuming a linear velocity profile inside the liquid film (Couette shear-driven flow) and taking into account the stability parameter (ζ):

$$h_c = 0.0288 \frac{c_c}{Pr_c^{0.667} \mu_c^{0.2} x^{0.2}} \left(\frac{\zeta W_c u_g h_g Pr_g^{0.667} \rho_c}{\pi r c_g} \right)^{0.4} \tag{6}$$

In NASA SP-8124 report,[6] two film cooling analytical models are proposed. One deals with LFC, and the second with GFC. In this discussion, only LFC is of relevance. The evaluation of film effectiveness (η) is evaluated, from the

LIQUID FILM COOLING ANALYSIS

knowledge of the LFC, with the aim of computing the adiabatic wall temperature (T_{aw}) beneath. The covered length has the usual definition, assuming the following expression:

$$L_c = \frac{1}{A_{ent}} \ln\left(1 + \frac{A_{ent}\, W_c}{V}\right) \tag{7}$$

In Eq.7, W_c is the film coolant flow rate in lbm/s, V is the vaporization rate of the liquid surface and A_{ent} is the liquid entrainment parameter, function of X_p, the entrainment correlation parameter (defined in Eq. 8).

$$X_p = \frac{\gamma \left(\frac{\rho_g}{g}\right)^{0.5} u_g \left(\frac{T_g}{T_{lf}}\right)^{0.25}}{\rho_{g,surf}} \tag{8}$$

The variable appearing in Eq. 8 are:

- T_g: core flow temperature;

- T_{if}: liquid interface temperature;

- γ: empirical augmentation factor, considering injection effects;

- ρ_g: core flow density;

- u_g: core flow velocity;

- $\rho_{g,surf}$: core flow surface density;

The wall temperature beneath the liquid coolant can be retrieved from the knowledge of the liquid film cooling effectiveness, whose definition derives from:

$$\eta = \frac{T_{aw} - T_g}{T_c - T_g} \tag{9}$$

Yielding to:

$$\eta = \frac{1}{\theta\left(1 + \frac{W_e}{W_c}\right)}, \qquad \frac{W_e}{W_c} = \frac{W - W_c}{W_c}\left[2\,\psi_L \frac{\bar{z}}{r_i}\sqrt{1 - \frac{(W_e)_{L_c}}{W - W_x}} - \left(\psi_L \frac{\bar{x}}{r_i}\right)\right] + \frac{(W_e)_{L_c}}{W_c} \tag{10}$$

Where it is possible to notice a dependence on the core stream and coolant flow rates (W_g, W_c), the amount of entrained coolant mass fraction (W_e/W_c) and the effective contour distance downstream of the injection ($\bar{z}$) responsible for the 2D effects of the chamber. Besides the evaluation of the entrained mass fraction, the effectiveness assessment passes through the calculations of the mixing layer structure profile parameter θ:

$$\theta = \begin{cases} 0.6 + 0.263\left(\dfrac{W_g - \left(W_g\right)_{L_c}}{W_c}\right) & W_g < \left(W_g\right)_{L_c} + 0.6\,W_c \\[3mm] 0.758 & W_g \geq \left(W_g\right)_{L_c} + 0.6\,W_c \end{cases} \tag{11}$$

At this stage, from the knowledge of the effectiveness, the adiabatic wall temperature is now computed, considering a non-reacting mixing layer:

$$T_{aw} = \frac{H_{aw} - \eta H_{c,sv} + \eta c_{Vap} T_{if} + (1 - \eta)(c_g T_{tot,g} - H_g)}{\eta c_{Vap} + (1 - \eta)c_g} \tag{12}$$

The unique unknown in Eq. 12 is the adiabatic wall enthalpy, whose expression has the following form:

$$H_{aw} = H_{tot,g} - \eta\left(H_{tot,g} - h_c\right) - \left(1 - Pr_w^{0.333}\right)\left(H_{tot,g} - H_g\right) \tag{13}$$

Thus, similarly to Stechman's approach,[29] the wall temperature beneath the film is evaluated, stating the constraints for the very same value.

Differently from the previous two models, Grissom[9] proposes a 1-D approach for the evaluation of the length at which the liquid layer still endures in liquid form. The model marches on the engine axis, monitoring the evolution of the coolant flow rate and temperature, before and after the saturation point of the same. The following hypotheses are considered:

- Steady state flow;

- Adiabatic film-wall interface;

- Non-reacting coolant stream and diffusion process;

- Steady and uniform core gas temperature.

Energy, mass, and momentum balances allow for the tracking of temperature (T_C), coolant flow rate (Γ_C), thickness (δ_C), and velocity (u_C), respectively. Starting from the energy balance at the liquid film bore surface, the temperature is tracked in space by:

$$\frac{dT_c}{dx} = \frac{\dot{q}''_{Tot}}{\Gamma_c \, C_{P,c}} \tag{14}$$

In the first portion of the model (i.e., the pre-saturation conditions), the coolant is studied from the point at which it is injected into the chamber till the saturation point. The total heat flux ($\dot{q}''_{Tot}$) from the mainstream gas, is the sum of convection and radiation heat fluxes:

$$\dot{q}''_{Tot} = \dot{q}''_{Conv} + \dot{q}''_{Rad}, \qquad \dot{q}''_{Conv} = h_0(St)\left(T_g - T_c\right), \qquad \dot{q}''_{Rad} = \sigma \, \epsilon \, \alpha_w \left(T_g^4 - T_c^4\right) \tag{15}$$

Where the convective heat transfer is expressed via the Reynolds analogy. Stanton number and friction factor correlations are employed considering a turbulent motion stream, flowing over a flat plate, and corrected for thrust chamber curvature. As far as concerns the radiation heat flux, the emittance of the exhausted mixture is evaluated taking into consideration the composition of the exhausted stream, following the approach suggested by Siegel and Howell.[12]
In Eq. 14, Γ_c is the coolant mass flow rate per unit circumference, constant till the saturation point. Once this point is reached, the temperature of the coolant remains constant, equal to the saturation one, and the coolant flow rate per unit circumference varies accordingly, as an effect of evaporation:

$$\frac{d\Gamma_c}{dx} = -\dot{m}''_{Evap}, \qquad \dot{m}''_{Evap} = \frac{\dot{q}''_{Tot}}{\lambda_{LHV}} \tag{16}$$

In Eq. 16, λ_{LVH} is the coolant latent heat of vaporization. As an effect of the evaporation process, the coolant mass, now in the gaseous state, leaves the thin liquid film slowly diffusing in the core stream flow. In this way, the convection heat transfer coefficient is largely reduced.[9] Grissom computes such a new coefficient implicitly, as a function of the evaporated mass. Proceeding with the integration, Γ_c reduces monotonically until it reaches a null value, this new position identifies as the film-cooled length (L_c, FCL).
In addition to this, the model includes the evaluation of the liquid film thickness and the average velocity both before and after the reaching of the saturation conditions, employing a laminar Couette flow. Introducing the momentum conservation equation, both the velocity and thickness can be related to Γ_c and to the surface shear stresses:

$$\begin{cases} \dfrac{d^2 u_c}{dy^2} = 0, \qquad u_c(0) = 0, \qquad \left(\dfrac{du_c}{dy}\right)_{x=\delta_c} = \dfrac{\tau}{\mu_c} \\[2mm] \Gamma_c = 2\, u_c\, \rho_c\, \delta_c \\[2mm] \tau = \dfrac{1}{2} c_f P_d \end{cases} \tag{17}$$

Differently from the others, Grissom does not directly account for the mass loss as an effect of entrainment. In his modeling procedure, an empirical correlation for film stability is provided as a function of core stream and coolant viscosity. No quantitative evaluation of the mass loss due to entrainment is provided, nor discussed.
The model developed by Shine[27] allows for the evaluation of the length at which the film still exists in the liquid state, and it is not completely evaporated. Employing the very same set of hypotheses of Grissom,[9] and the control volume depicted in Fig. 1. Global energy and mass balances are retrieved for the film-cooled length evaluation. In this framework, differently from Grissom, the FCL is evaluated via a lumped-parameter approach, without considering an effective integration procedure. The mass balance equation is written as:

$$\dot{m}_c = \dot{m}_{c,Evap} + \dot{m}_{c,Entr} \tag{18}$$

Whereas, the energy balance takes the form:

$$\dot{m}''_{c,Evap}\, h^*_{f,g} = \dot{q}''_{Conv} + \dot{q}''_{Rad} \tag{19a}$$

5

LIQUID FILM COOLING ANALYSIS

With:

$$h_{fg}^* = h_{fg,c} + (T_{sat} - T_{inj})c_c \tag{19b}$$

Where, in Eq. 18, $\dot{m}_c$ is the total injected mass flow rate of coolant that can be lost by vaporization ($\dot{m}_{c,Evap}$) and entrainment ($\dot{m}_{c,Entr}$). As per Eq. 19a and Eq. 19b, the total input heat flux, responsible for the vaporization mass loss contribution, is the sum of the convection ($\dot{q}_{Conv}''$) and radiation ($\dot{q}_{Rad}''$) input heat fluxes. The vaporized mass loss is evaluated via a modified enthalpy of vaporization (h_{fg}^*) containing: the effective enthalpy of vaporization ($h_{fg,c}$) and the contribution to enhancing its temperature till the saturation value.

Moving further, the Darcy friction factor and the Stanton number are evaluated according to McKeon et al.,[22] and Friend-Metzner,[30] respectively. Both correlations are suitable for fully developed pipe flow, differently from what is pursued by Grissom,[9] (valid for $300 \cdot 10^3 \le Re_D \le 18 \cdot 10^6$).

$$\frac{1}{\sqrt{C_f}} = 1.930 log(Re_D \sqrt{C_f}) - 0.537 \tag{20}$$

$$St = \frac{\frac{f}{2}}{1.20 + 11.8 \sqrt{\frac{f}{2}}(Pr-1)(Pr)^{-\frac{1}{3}}}, \qquad f = \frac{C_f}{4} \tag{21}$$

Considering the problem in its global formulation, the St shall be modified accordingly, taking into account the transpiration effects. Thus, defining the St in the absence of mass blowing as St_0, the following relations hold:

$$\frac{St}{St_0} = \frac{\ln\left[1 + (F/St)\left(MMol_g/MMol_c\right)^{0.6}\right]}{(F/St)\left(MMol_g/MMol_c\right)^{0.6}} \tag{22a}$$

$$\frac{F}{St} = \frac{c_g}{h_{fg}^*}\left[\left(T_g - T_{sat}\right) + \frac{\dot{q}_{rad}''}{h}\right] \tag{22b}$$

Meinret[23] proposed a correlation based on the Stanton Number, which paired with Eq. 22b involving the blowing ratio (F/St), leading to the evaluation of the convection heat transfer coefficient implicitly, and the relative heat flux. Concerning the radiation heat flux, its evaluation is possible via the implementation of Leckner's[19] correlation for the emissivity. Knowing the two input heat flux contributions and the modified vaporization enthalpy, the evaporation mass flux may be evaluated as follows:

$$\dot{m}_{c,Evap}'' = \frac{\dot{q}_{Tot}''}{h_{fg}^*} = \frac{\dot{q}_{Conv}'' + \dot{q}_{Rad}''}{h_{fg}^*} \tag{23}$$

Differently from the previous works, the film instability is investigated, and the relative fraction of mass loss is evaluated. The film is made unstable as an effect of the existence of large-scale disturbances which engenders the generation of roll waves on the film bore surface, and its possible droplet mechanical detachment.[27,28] The entrainment mass fraction (E) is introduced using the Sawant et. al[26] correlation, via the Weber number (We).

$$E = E_m \tanh\left(a_c We^{1.25}\right), \qquad a_c = 2.31 \cdot 10^{-4} Re_c^{-0.35} \tag{24a}$$

$$E_m = 1 - \frac{Re_{c,film}}{Re_c} \tag{24b}$$

$$Re_{c,film} = 250 \ln(Re_c) - 1265 \tag{24c}$$

$$We = \frac{\rho_g u_g^2 D_c}{\sigma \left(\Delta\rho/\rho_g\right)^{1/4}} \tag{24d}$$

From the knowledge of the injected coolant flow rate (expressed as the coolant flow rate per unit circumference, Γ_c), curtailed by the entertainment mass losses and (evaluated via Eq. 24a), and the contribution of mass deficit due to vaporization, the length for which the liquid persists in liquid form is evaluated as:

$$L_c = \frac{\Gamma_c}{\dot{m}_{c,Evap}''} = \frac{1}{\dot{m}_{c,Evap}''} \frac{\dot{m}_c - \dot{m}_{c,Ent}}{2\pi r_{cc}} \tag{25}$$

3. Analytical Film Cooling Model Development

In the present section, the new model for film cooling (S1D) is developed and discussed in detail. In the beginning, preliminary considerations on pre-existing models are performed, to define a starting point for its development, exploiting consolidated hypotheses and modeling techniques. Later on, the S1D model is described, starting from its simplified version for which no entrainment is considered. As a last step, the S1D version including entrainment is described.

3.1 Preliminary Considerations

The models presented in Ref.[29] and Ref.[6] allow for the evaluation of the temperature beneath the film in steady conditions, employing global balances. Whereas, the model developed by Grissom[9] foresees the evaluation of the FCL (Film Cooled-Length) employing local mass and energy balances as outlined in Eq. 14 and Eq. 16, however no clue about the film hydrodynamic stability is provided nor discussed. The model presented by Shine[27] exploits global mass and energy balances for the evaluation of the protected area, also in the presence of potential liquid-film destabilizing agents as the core stream, in fact, the mass losses due to entrainment are directly assessed.

The aim of the present article is to derive a more generalized version of the film cooling model starting from the 1D version of Ref.[9] Therefore, local mass and energy balances are employed, in parallel to a more precise and exhaustive description of all the phenomena occurring in the thrust chamber. Particular emphasis is dedicated to the shearing action exerted by the core stream onto the thin liquid film. In fact, a much more precise treatment of the entrainment phenomenon is fulfilled, borrowing from the Hybrid Rocket Engines (HREs) background in liquefying fuels.[14]

3.2 Simplified Model Architecture, S1D-V0

The model here developed follows the efforts made by Grissom,[9] hence a 1D space marching scheme is derived. The coupled energy, mass, and momentum balances are solved for both the pre-saturation and post-saturation conditions. The marching scheme moves along the longitudinal axis of the engine, labeled as the x-axis, while the orthogonal planar direction is defined as the y-axis.

Starting from the energy and mass balances, the coolant temperature and the flow rate per unit circumference are tracked along the engine axis, once it is subjected to a high enthalpy core stream. The latter raises the coolant temperature via convection and radiation, up to the saturation value. At this point, the thin film starts losing mass, constant up to this condition, as an effect of the aggregation phase transition. Assuming a pure laminar regime for the coolant, a shear-driven flow is exploited for the motion description of the same. Hence, from a simple Couette flow, the velocity and the thickness of the coolant are assessed, in conjunction with the magnitude of the exerted shear stresses.

Considering the liquid film control volume depicted in Fig. 2, the liquid coolant is subjected to an enthalpy flux deriving from the high-temperature core stream (T_g). Assuming a flat plate geometry and relative correlations, corrected for the chamber curvature, the following set of equations is defined for the pre-saturation conditions:

$$\begin{cases} \dfrac{dT_L}{dx} = \dfrac{\dot{q}''_{Tot}(x)}{\Gamma_L(x)\,C_{P,L}(T)} = \dfrac{1}{\Gamma_L(x)\,C_{P,L}(T)}\left[\dot{q}''_{Rad}(x) + \dot{q}''_{Conv}(x)\right] \\[2mm] \dfrac{d\Gamma_L}{dx} = 0 \\[2mm] \Gamma_L(x) = 2\,\rho_L(T)\,u_L(x)\,\delta_L(x) \\[2mm] \dfrac{d^2 u_L(x)}{dy^2} = 0, \qquad u_L(x,0) = 0, \qquad \mu_L(T)\,\dfrac{du_L(x)}{dy}\bigg|_{y=\delta_L(x)} = \dfrac{1}{2}\,C_f\,P_D \end{cases} \tag{26}$$

Primarily focusing on the convection heat flux, the relative heat transfer coefficient is derived from the knowledge of the St_0 and the C_f, via the Reynolds analogy typical for flat plates and augmented for the turbulent motion regime.[3,25] The latter influence is included by the K_{Tu} (a parameter dependent on the turbulence intensity), hence:

$$\dot{q}''_{Conv}(x) = h_0(x)\left(T_g - T_L(x)\right) \tag{27a}$$

$$h_0(x) = K_{Tu}\,G_{Avg}(x)\,C_{P,g}\,St_0(x) \tag{27b}$$

$$St_0(x) = \frac{1}{2}\,C_f(x)\,Pr^{-0.667} = \frac{Pr^{-0.667}}{2}\left[0.0592\,Re_x(x)^{-0.2}\right] \tag{27c}$$

LIQUID FILM COOLING ANALYSIS
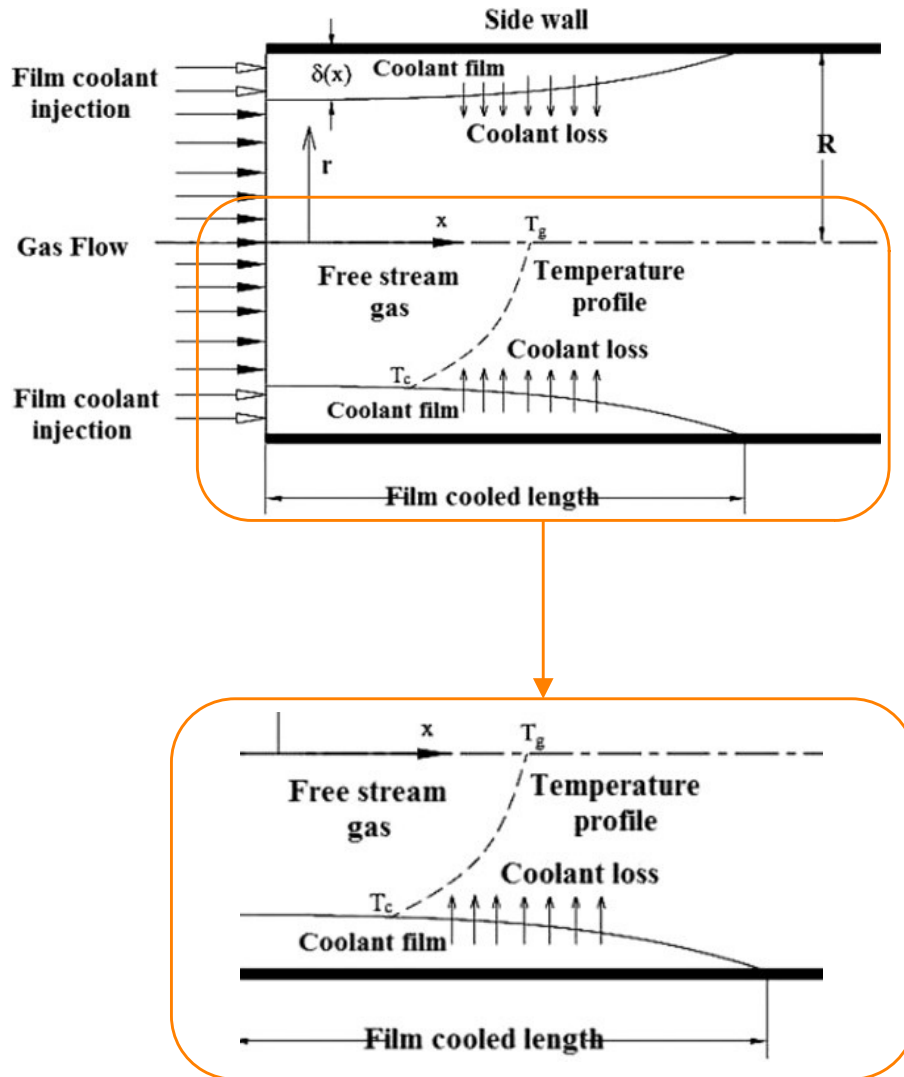
Figure 2: S1D model, FC control volume (original image after adaptation from Ref.[27]).

$$G_{Avg}(x) = \rho_g u_g \left(\frac{2 T_g}{T_g + T_{L,Sat}} \right) \left[\frac{u_g - u_{L,Surf}(x)}{u_g} \right] \tag{27d}$$

As far as concerns the radiation heat flux, the following formulation is employed:

$$\dot{q}''_{Rad}(x) = \sigma A_w \epsilon \left(T_g^4 - T_L^4(x) \right) \tag{28}$$

Where the emittance of the exhausted mixture (ϵ) is evaluated via an interpolation process, as suggested by Siegel and Howell.[12]

Having defined all the parameters in the system Eq. 26, the integration procedure may start, from the injection point labeled with $x = 0$, until a specific stopping criterion is matched: $T_L(\overline{x}) = T_{L,Sat}$. Once this condition is verified, the saturation point is reached, the coolant starts evaporating, and the previous system of equations modifies accordingly:

$$\begin{cases} \dfrac{dT_L}{dx} = 0, \qquad T_L(x > \overline{x}) = T_{L,Sat} \\[2mm] \dfrac{d\Gamma_L}{dx} = -\dot{m}''_{Evap}(x) \\[2mm] \Gamma_L(x) = 2 \rho_L(T_{L,Sat}) u_L(x) \delta_L(x) \\[2mm] \dfrac{d^2 u_L(x)}{dy^2} = 0, \qquad u_L(x,0) = 0, \qquad \mu_L(T_{L,Sat}) \dfrac{du_L(x)}{dy}\bigg|_{y=\delta_L(x)} = \dfrac{1}{2} C_f P_D \end{cases} \tag{29}$$

As presented in Eq. 29, the temperature is constant and equal to the saturation one, whereas the liquid coolant starts transpiration, thus hot vapors leave the liquid coolant, diffusing in the mainstream. This procedure has a further impact on the overall convection heat transfer: mass blowing from the coolant layer reduces the convection heat transfer (as well as the surface friction). In this framework, the production of hot vapors generates a buffer layer obstructing and drastically reducing the convection heat transfer, as largely witnessed and assessed in hybrid rocket propulsion.[20, 21] The mass flux of evaporated coolant is evaluated as the ratio of the total input heat flux and the enthalpy of vaporization (λ_{LHV}):

$$\dot{m}''_{Evap}(x) = \frac{\dot{q}''_{Tot}(x)}{\lambda_{LHV}} = \frac{\dot{q}''_{Conv}(x, T_{L,Sat}) + \dot{q}''_{Rad}(x, T_{L,Sat})}{\lambda_{LHV}} \tag{30a}$$

$$\dot{q}''_{Rad}(x, T_{L,Sat}) = \sigma A_w \epsilon \left(T_g^4 - T_{L,Sat}^4(x) \right) \tag{30b}$$

$$\dot{q}''_{Conv}(x, T_{L,Sat}) = h(x) \left(T_g - T_{L,Sat}(x) \right) \tag{30c}$$

This reduction is assessed via the so-called blowing ratio H, and accounting for the difference in the molar masses between the exhausted stream and the coolant hot vapors (included in the K_M coefficient):

$$h(x) = h_0(x) \ln \left(\frac{1 + H}{H} \right) \tag{31a}$$

$$H = C_{P,g} K_M \frac{\dot{m}''_{Evap}(x)}{h(x)} \tag{31b}$$

Having defined all the parameters in Eq. 29, the integration procedure may be resumed under the new specified conditions, from point $\overline{x}$ (saturation) until all the liquid coolant mass has completely evaporated. This point ($\Gamma_L = 0$) is marked as film-cooled length or FCL.

The S1D/V0 model is coded in a MATLAB environment, following the scheme depicted in Fig. 3:

3.3 Film Hydrodynamic Stability Assessment

At this stage, the basic version of the present model is outlined, hence no clue about the hydrodynamic stability of the liquid film is discussed or investigated. Concerning all the other models, Ref.[29] and Ref.[6] cover the film stability, nonetheless, mere rules of thumb and empirical relations are provided. In this groundwork, a pre-multiplying coefficient is retrieved, whose value is bounded between 0 and 1. In addition to this, Ref.[9] does not cover explicitly the stability of thin films, recalling the empirical relation provided by Knuth,[18] where instability is triggered whenever a critical ratio is overcome. The latter is dependent upon the core stream and coolant viscosity. Reference,[27] instead, provide a
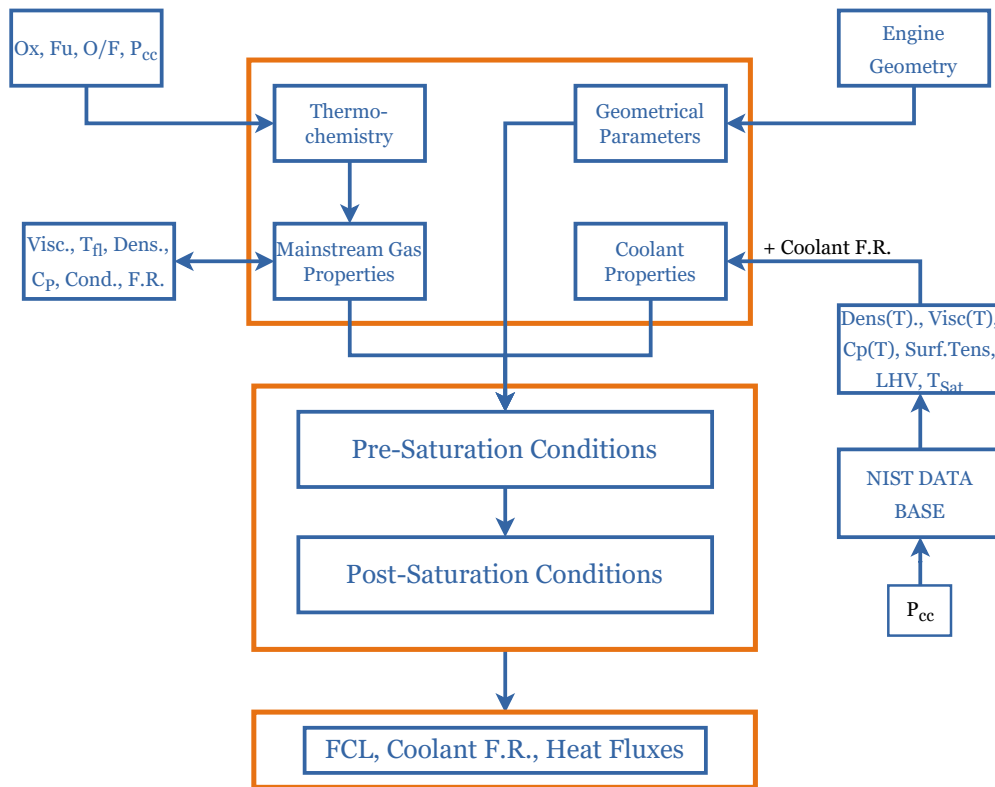
LIQUID FILM COOLING ANALYSIS

Figure 3: S1D code flow chart.

more rigorous treatment for film instability, based on the Weber number. Moreover, a relation for the evaluation of the fraction of entrained mass is presented, from Sawant.[26]

In S1D/V0, the contribution of entrainment is introduced and deeply investigated. Following the works of Gater and l'Ecuyer[7] and of Karabeyoglul,[14] film stability is discussed in detail. Recalling the two works, the thin film is subjected to a shearing action by the core stream, hence roll waves may generate on the free surface of the same, as an effect of exhausted gases dynamic pressure. The generation of the roll waves may not directly provokes the detachment of liquid droplets, whenever the inertia forces superclass the retention forces via the liquid surface tension.

The phenomenon discussed above is similar to the one depicted in Fig. 4, though the latter comes from the analysis of a liquid layer on a solid substrate, a condition typical of HREs with liquefying fuels. Therefore, a duplex can be witnessed, in fact in conjunction with a mass loss before and after the reaching of the saturation process, an enhanced roughness on the film free surface is present. The latter has a direct impact on the convection mechanism, in fact, the increased surface roughness largely increases the convective heat flux towards the film surface.

Having understood the concerns related to the entrainment phenomenon, a thorough analysis shall consider:

- Understanding whether the film may be made unstable under a shearing action. Hence, an inception criterion for entrainment shall be outlined;

- Evaluation of the mass loss as an effect of induced shearing action;

- Assessment of the increased free surface roughness and its impact on the convective heat transfer coefficient

These points are accomplished with the works of Gater and Karabeyouglu, for which an inception criterion is defined depending on the dynamic pressure of the core stream, the coolant mass loss is evaluated as a function of the thickness of the same and also the increased roughness (Fr) value of the free surface. The latter is then introduced onto the convective heat transfer coefficient in the following way, as suggested by Bons:[2]

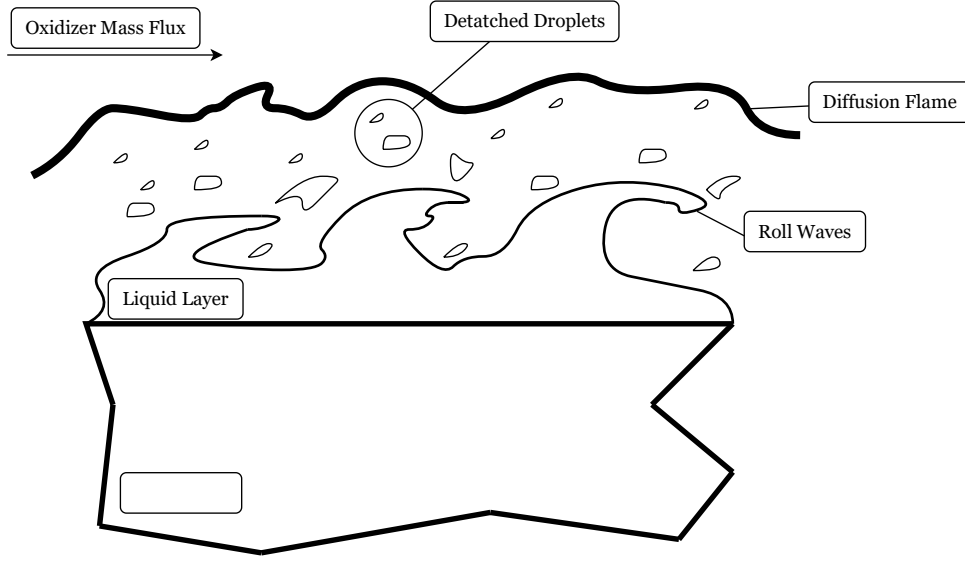$$\frac{2\,St(x)}{Cf(x)} \;=\; Pr^{-0.667}\,[1 + Fr(x)] \tag{32}$$

10

Figure 4: HRE entrainment schematic mechanism.

3.4 Complete Model Architecture, S1D/V1

Having consolidated the architecture of the model outlined in Sec. 3.2 and in Fig. 3. The contribution of entrainment is introduced in Eq. 26 and in Eq. 29, whenever an onset criterion for this phenomenon is triggered. Such a threshold for the enhanced mass transfer due to entrainment is given as:

$$X_e \geq 2109, \qquad X_e = \frac{P_D^{0.5}}{\sigma_L(T)\left(T_g/T_{L,Sat}\right)^{0.25}} \tag{33}$$

Where X_e is defined as the entrainment parameter according to Karabeyoglu,[14] recalling the experimental data set and post-processing by Gater.[7] Whenever the X_e parameter is greater than the threshold of Eq. 33, entrainment is triggered and droplets may detach from the liquid film-free surface. The loss in mass due to the mechanical shearing action is evaluated as follows:

$$\dot{m}''_{Ent}(x) = 1.41 \cdot 10^{-3} \left(X_e - 2109\right) \dot{m}''_{Cool}(x) \tag{34a}$$

$$\dot{m}''_{Cool}(x) = \frac{P_D\, C_f(x), \delta_L^2(x)\, \rho_L(T)}{2\,\mu(T)} \tag{34b}$$

At this stage, also the roughness is evaluated, following the treatment of Ref.,[14] thus:

$$Fr = \frac{14.1\,\rho_g^{0.4}}{G_g^{0.8}\left(T_g/T_{L,Sat}\right)^{0.2}} \tag{35}$$

Having understood the modeling procedure for the new actors involved whenever entrainment is introduced, the systems of equations for the pre-saturation conditions, defined in Eq. 26, are modified as follows:

$$
\begin{cases}
\dfrac{dT_L}{dx} = \dfrac{\dot{q}''_{Tot}(x)}{\Gamma_L(x)\, C_{P,L}(T)} = \dfrac{1}{\Gamma_L(x)\, C_{P,L}(T)}\left[\dot{q}''_{Rad}(x) + \dot{q}''_{Conv}(x)\right] \\[2ex]
\dfrac{d\Gamma_L}{dx} = -\dot{m}''_{Ent}(x) \\[2ex]
\Gamma_L(x) = 2\,\rho_L(T)\, u_L(x)\, \delta_L(x) \\[2ex]
\dfrac{d^2 u_L(x)}{dy^2} = 0, \qquad u_L(x,0) = 0, \qquad \mu_L(T)\left.\dfrac{du_L(x)}{dy}\right|_{y=\delta_L(x)} = \dfrac{1}{2}\,C_f\,P_D
\end{cases} \tag{36}
$$

LIQUID FILM COOLING ANALYSIS

In the post-saturation conditions, the same equations in system Eq. 29 adapts accordingly. Hence in the presence of entrained mass:

$$
\begin{cases}
\dfrac{dT_L}{dx} = 0, \qquad T_L(x > \overline{x}) = T_{L,Sat} \\[2mm]
\dfrac{d\Gamma_L}{dx} = -\dot{m}''_{Evap}(x) - \dot{m}''_{Ent}(x) \\[2mm]
\Gamma_L(x) = 2\,\rho_L(T_{L,Sat})\,u_L(x)\,\delta_L(x) \\[2mm]
\dfrac{d^2 u_L(x)}{dy^2} = 0, \qquad u_L(x,0) = 0, \qquad \mu_L(T_{L,Sat})\,\dfrac{du_L(x)}{dy}\bigg|_{y=\delta_L(x)} = \dfrac{1}{2}\,C_f\,P_D
\end{cases}
\tag{37}
$$

In both situations, in the presence of entrainment, the convection heat transfer coefficient varies as suggested in Eq. 32. Hence, for both pre-saturation and post-saturation conditions, the following formulations hold:

$$
St_0^{Ent}(x) = \frac{1}{2}C_f(x)\,Pr^{-0.667}\,(1 + Fr)
\tag{38a}
$$

$$
h_0^{Ent}(x) = K_{Tu}\,G_{Avg}(x)C_{P,g}\,St_0^{Ent}(x) = K_{Tu}\,G_{Avg}(x)C_{P,g}\,St_0(x)\,(1 + Fr)
\tag{38b}
$$

$$
h^{Ent}(x) = h_0^{Ent}(x)\,\ln\left(\frac{1+H}{H}\right) = h_0(x)\,(1 + Fr)\,\ln\left(\frac{1+H}{H}\right)
\tag{38c}
$$

4. Model Validation and Results

The results of the S1D film cooling model are presented and discussed in this section. As a first step, the results deriving from a specific data set are outlined. Such a data set is exploited as a benchmark for understanding the film cooling ruling mechanisms.

First, the results of S1D in the absence of entrainment are presented and discussed. Later on, the validation process for the entrainment phenomenon is carried out, using the large data set from Gater. Further, the outcomes, considering the entrainment, are considered contrasting them with respect to the one from S1D/V0. As a last consideration, the model for film cooling is largely validated using three different data sets:

- Morrel data set,[24] a LRE using LOX-LNH$_3$ as propellant couple and water as coolant. Four different tests are replicated, namely tests: MT8-MT9-MT10-MT11. With MT8 being the benchmark test for the early analyses;

- Kinney data set,[15] an exhausted mixture of gasoline-air flowing in a fixed diameter duct. Water is employed as a coolant. Four tests are replicated: KiT1-KiT2-KiT3-KiT4;

- Knuth data set,[18] a stream of heated air, flowing in a 2.9" diameter duct, using water as coolant. Four tests are replicated: KnT20-KnT45-KnT89-KnT109;
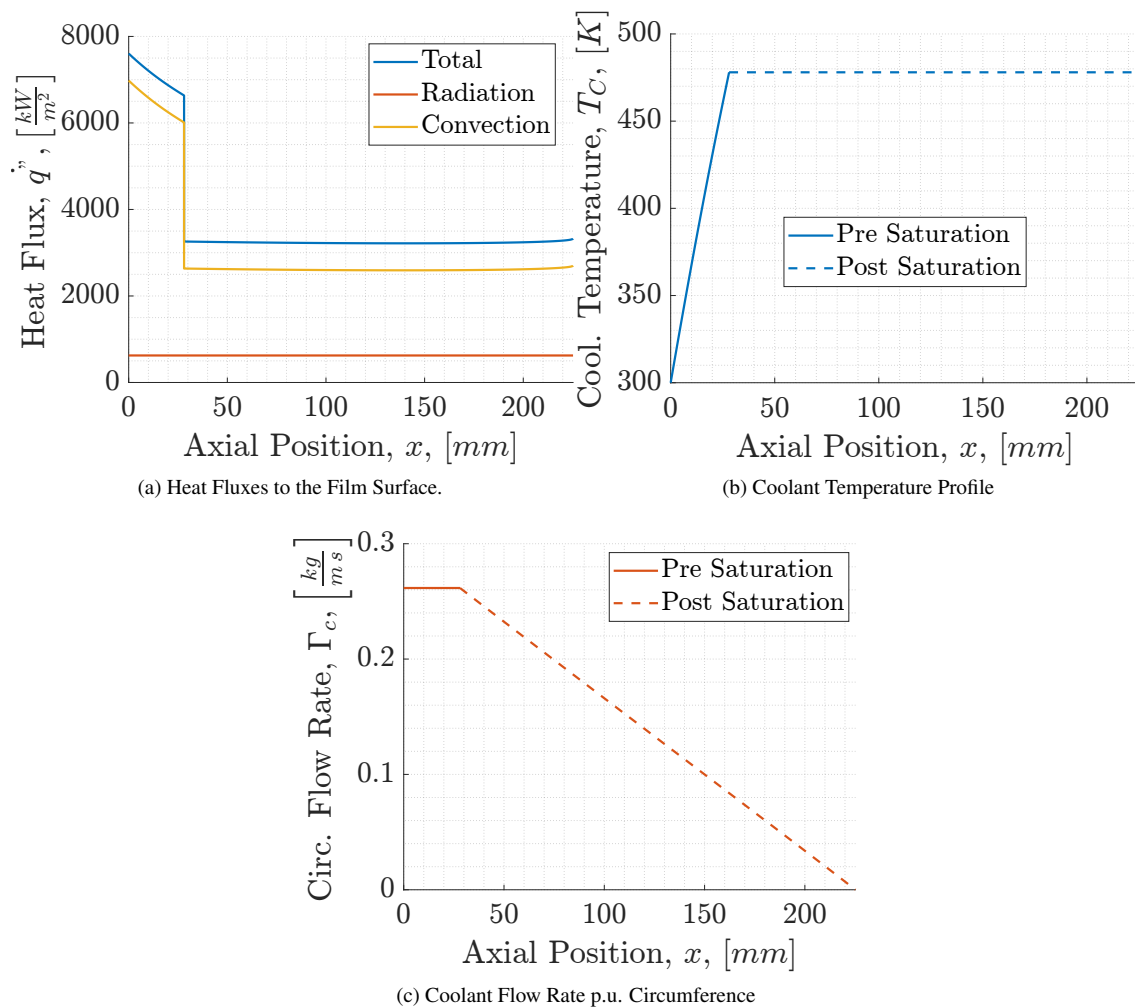
4.1 S1D/V0 Model Results

The results deriving from S1D/V0 for Morrel's test-8 are presented hereby, in the framework of understanding the physical mechanisms behind film cooling, and its impact on the thin film ruling parameters.

Preliminary considerations are carried out on the energy-mass-related parameters, such as heat fluxes reaching the coolant, its temperature, and flow rate per unit circumference (Γ_C). The latter is useful for assessing the liquid film-cooled length, the distance the Γ_C reaches a null value.

Looking at solid lines in Fig. 5c and Fig. 5b, the process for which the film absorbs enthalpy is justified. Temperature increases monotonically, hence decreasing the total heat flux, whereas the coolant flow rate is constant since no entrainment is considered. Once saturation conditions are reached, the temperature is constant and so is the heat flux. However, the coolant flow rate features a monotonically decreasing trend toward the null value. In this context, vaporization is triggered, hence the coolant starts evaporating producing hot vapors which have a positive effect on the incoming heat flux. As a consequence, the generation of fuel vapors physically obstructs the convection mechanism, drastically reducing the relative heat transfer coefficient, as suggested also in Eq. 31 via the blowing parameter H.

Further considerations can be inferred for the trends depicted in Fig. 6. The retrieved results concern the coupling between mass and momentum relations for the thin liquid coolant. In fact, the thickness, average velocity, and exerted shear stresses by the core stream are outlined.

(a) Heat Fluxes to the Film Surface.

(b) Coolant Temperature Profile

(c) Coolant Flow Rate p.u. Circumference

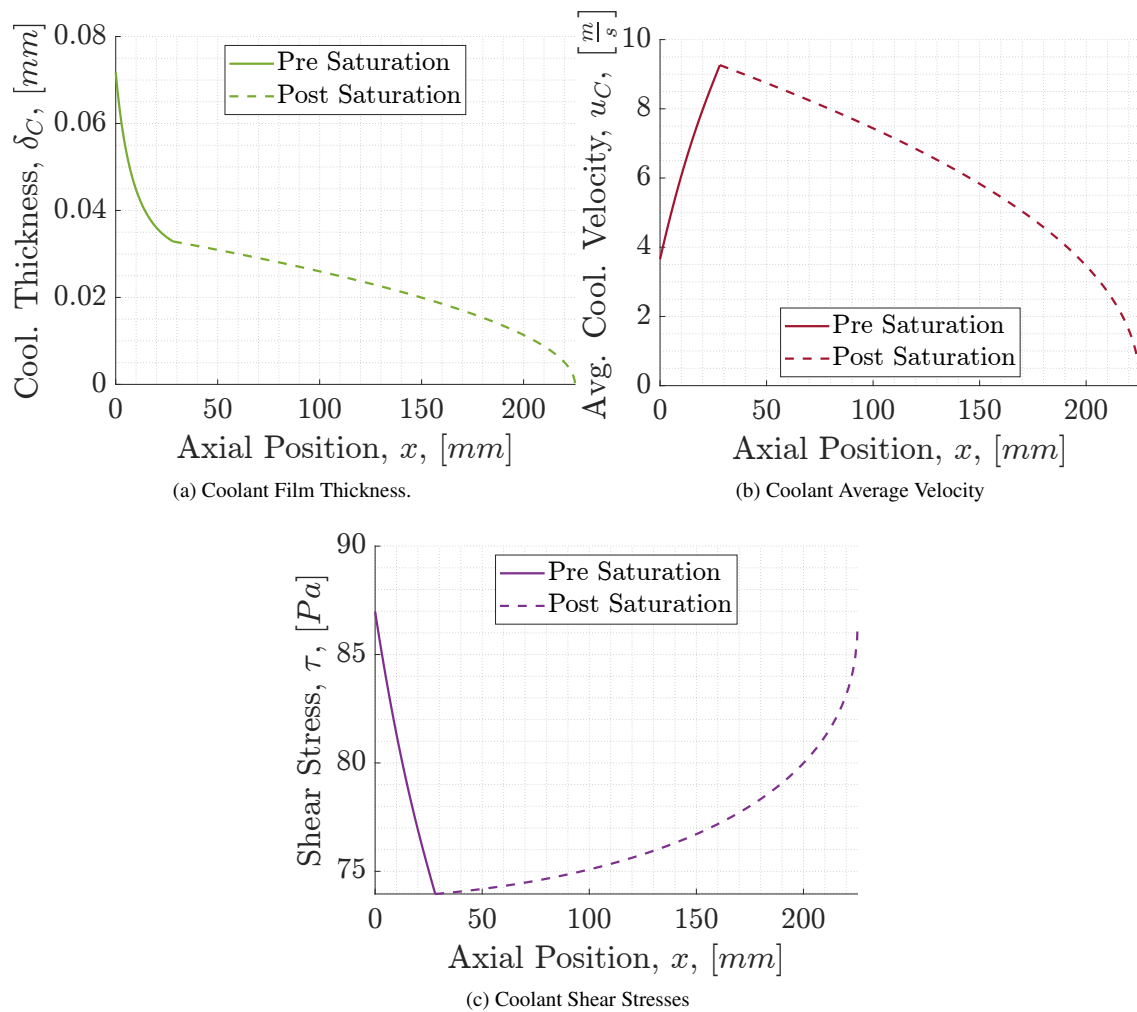Figure 5: Energy-Mass S1D/V0 Results, Morrel Test-8[24]

As it is possible to notice, the thickness varies with a monotonic decreasing trend as an effect of the vaporization, mainly, once saturation is reached. The average coolant velocity follows an opposite trend as an effect of the increased density during the pre-saturation condition, whereas a similar decreasing trend is followed during the post-saturation conditions: the density of the film is constant and the coolant flow rate is reducing, as a consequence of the vaporization process. Looking at the shear stresses, an adverse behavior with respect to velocity is found, as an effect of the relative motion between coolant and gas.

4.2 Entrainment Validation Process

The data set from Gater[7] is simulated for the entrainment validation process. In this framework, a flow of heated air ($400\,°F$, $477\,K$) is considered in a constant squared section, when methanol is injected close to the saturation temperature for cooling purposes. The amount of remaining mass is simulated at the fixed distance of 10" ($254\,mm$) downstream of its injector, and compared with the experimental findings. Air is accelerated from $89\,ft/s$ ($27.1\,m/s$) up to $287\,ft/s$ ($87.5\,m/s$), and methanol is introduced with mass flow rate spacing between $0.04\,lb/(ft·s)$ ($0.059\,kg/(m·s)$) and $0.20\,lb/(ft·s)$ ($0.30\,kg/(m·s)$). Hence a coolant flow rate per unit width (slit aperture) is considered.

The Fig. 7 depicts the comparison between the S1D model when only the entrainment effects are considered. Since the coolant temperature is close to the saturation, thus just entrainment may concur in the mass loss evaluation. Specifically, the S1D retrieved numerical-mass flow rates are compared to ones of Ref.,[7] when different values of injected coolant and different core stream velocities are considered. Looking at Fig. 7, the developed S1D model for film cooling, in the presence of a pure shearing flow, is able of predicting with a good level of accuracy the experimental results. Looking at the first two charts, namely 89-119 ft/s, S1D is capable of predicting the value of the retrieved mass flow rate with

LIQUID FILM COOLING ANALYSIS

(a) Coolant Film Thickness.

(b) Coolant Average Velocity

(c) Coolant Shear Stresses

Figure 6: Momentum-Mass S1D/V0 Results, Morrel Test-8[24]

a high level of accuracy. Instead, looking at the other charts, responsible for larger velocities, the prediction is still good at low values of injected coolant mass flow rate. The predictions diverge above $0.2\,kg/(m\,s)$, overestimating the entrainment mass loss mechanism.

4.3 S1D/V1 Model Results

In the present section, the results of the S1D/V1 model are presented, exploiting the same data set of Sec. 4.1. The latter model foresees the presence of entrainment, for which the system to be solved is modified according to Eq. 36 and Eq. 37.

Looking at the results gathered in Fig. 8, differences arise mainly in the coolant flow rate per unit circumference (Γ_C, see Fig. 8c) and in the heat fluxes reaching the film surface (Fig. 8a). In the first part of the chart of Fig. 8c a global monotonic decreasing trend is observed, in conjunction with a mild reduction of the coolant flow rate, prior to the saturation point. Hence, the unique mechanism for which mass may be removed is entrainment. This is also justified by the enhanced convection (thus total heat flux), as an effect of the increased roughness due to the roll waves mechanism.

All the previous considerations are better outlined in Fig. 10 and Fig. 11. The most evident difference lies in Fig. 10c, where the decreasing trend in the coolant flow rate is largely enhanced, and, as a consequence the FCL is largely curtailed. The latter reduces from an initial value of more than $225\,mm$ to a new value of $159\,mm$, marking a relative reduction of the $-29\,\%$.

Looking at the point for which the pre-saturation conditions are reached, a mild anticipation of the phenomenon is witnessed in Fig. 10b. As a further consideration, Fig. 10a precisely marks the augmented convection heat transfer due

14
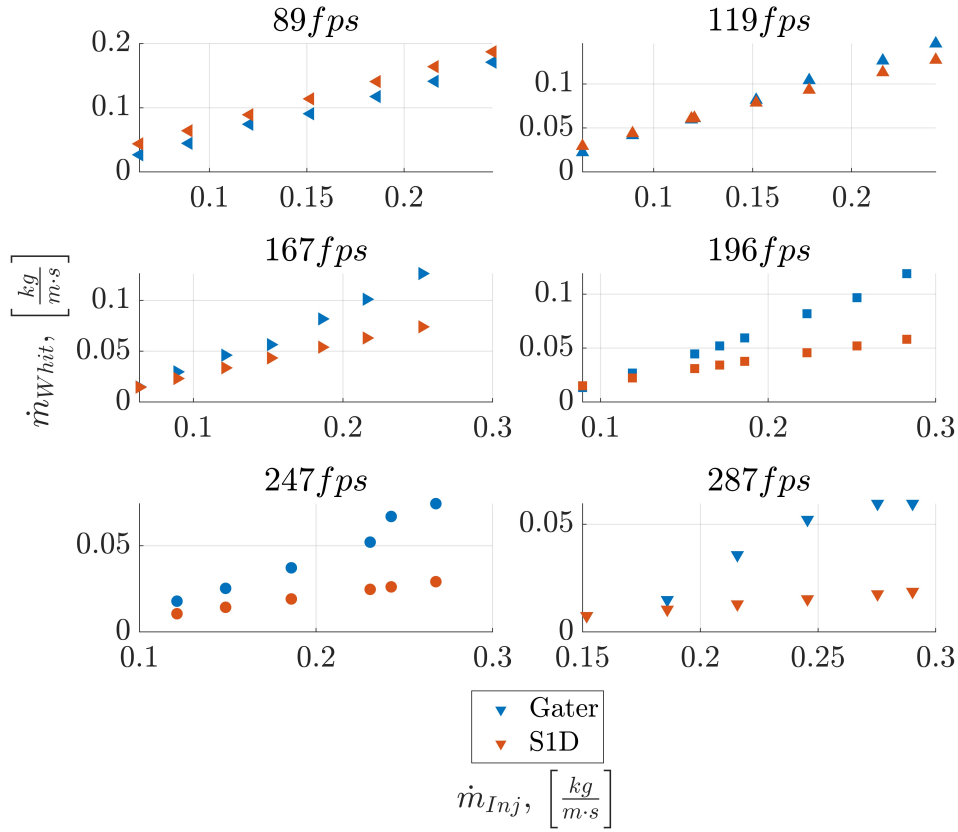
Figure 7: S1D/V1 validation of entrainment results.[7]

to the aforementioned reasons. The peak value at the beginning of the film is enhanced by approximately the +11 %, however, the convection heat flux, when entrainment is considered, is generally higher with respect to its counterpart, when this peculiar mechanism is not conceived.

The effects of entrainment are also highlighted in the results grouped in Fig. 11. As it is possible to notice in Fig. 11a, the reduction in the thickness is most marked in the post-saturation region, as an effect of the largely reduced coolant mass fraction. As a consequence, also the coolant average velocity and the shear stresses are largely influenced. In fact, the velocity is experiencing a considerable reduction in conjunction with a largely enhanced shear stresses magnitude, as a further effect of the enhanced roughness for which also the friction factor is increased.
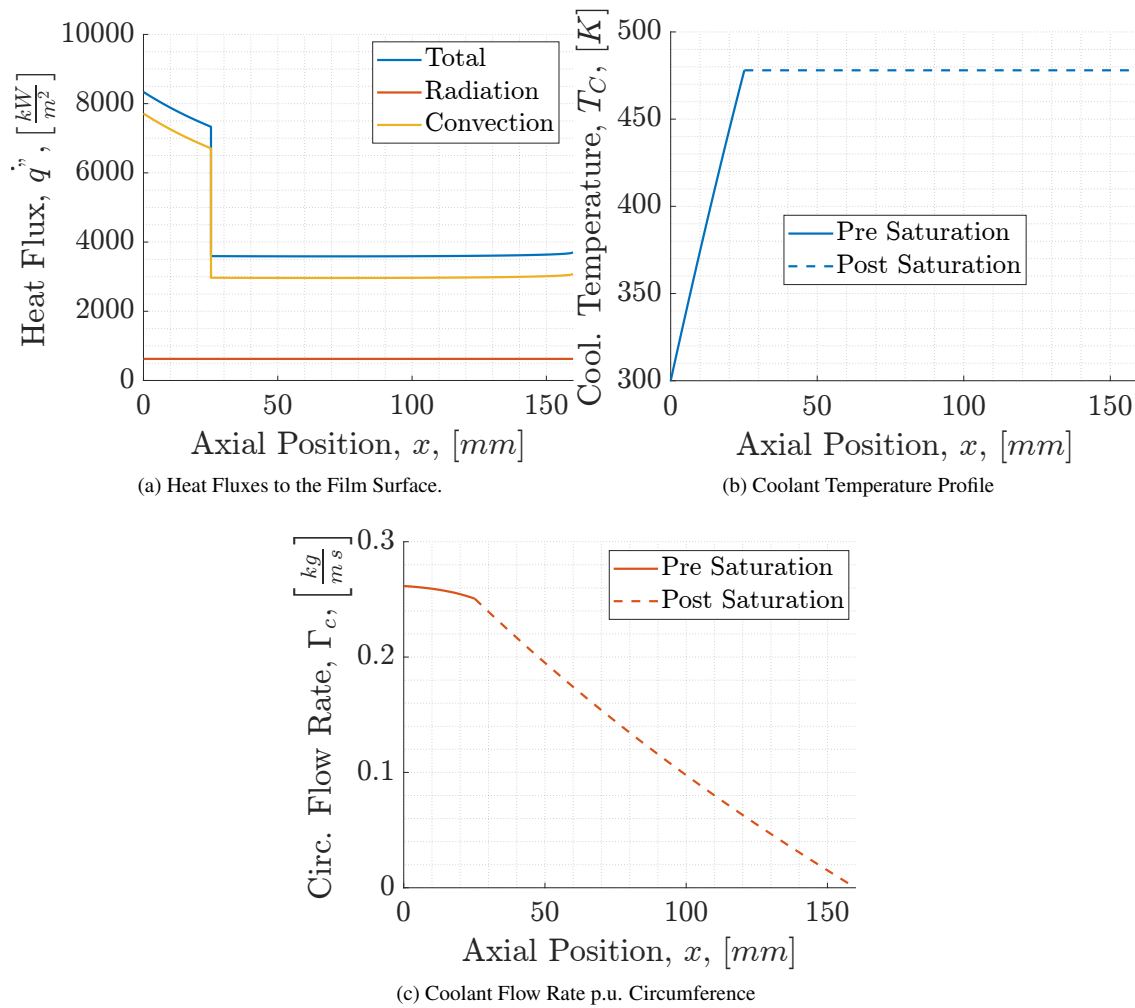
4.4 S1D Versus Morrel Data Set

In the present section, the S1D model is employed for simulating the Morrel data set.[24] Operating conditions for the considered tests MT8, MT9, MT10, and MT11 are gathered in Tab. 1. As it is possible to notice, different values of both core stream ($\dot{m}_g$) and coolant ($\dot{m}_c$) mass flow rates are considered, with a test pressure of $17\,bar$. Different oxidizer-to-fuel ratios are considered, spanning over 1.41-1.75 interval, for which the stoichiometric condition is met at $O/F = 1.41$.

Test ID.	$\dot{m}_g$ [kg/s]	$\dot{m}_c$ [kg/s]	P_{CC} [bar]	O/F [−]
MT8	1.689	0.0835	17.4	1.41
MT9	1.729	0.0835	17.1	1.51
MT10	1.820	0.0925	17.9	1.75
MT11	1.810	0.0943	17.9	1.67

Table 1: Operating conditions for tests from Ref.[24]

The results in Tab. 1 show the experimental FCL for each test. The experimental value is contrasted and compared

LIQUID FILM COOLING ANALYSIS

(a) Heat Fluxes to the Film Surface.

(b) Coolant Temperature Profile

(c) Coolant Flow Rate p.u. Circumference

Figure 8: Energy-Mass S1D/V1 Results, Morrel Test-8[24]

with respect to both the S1D/V0 and the S1D/V1 outputs. The experimental value for each test is recovered by means of thermo-couples measurement as reported in the Reference.[24]

Test ID.	Exp. *FCL* [mm]	Grissom *FCL* [mm]	Deviation [%]
MT8	188.0	246.0	+31
MT9	207.0	248.0	+20
MT10	204.0	277.0	+36
MT11	217.0	280.0	+29

Table 2: Results from the application of Grissom's model[9] to the tests from Ref.[24]

Test ID.	Exp. *FCL* [mm]	S1D/V0 *FCL* [mm]	Deviation [%]	S1D/V1 *FCL* [mm]	Deviation [%]
MT8	188.0	225.0	+20	159.0	-15
MT9	207.0	226.0	+9	159.6	-23
MT10	204.0	260.0	+27	176.9	-13
MT11	217.0	260	+20	176.8	-19

Table 3: S1D model results applied to Ref.[24] data set.

Looking at the reported results, focusing on the ones without the entrainment (S1D/V0), it is possible to notice a discrepancy between the model and the experimental findings. As witnessed, the simplified version of the film cooling

(a) Coolant Film Thickness.

(b) Coolant Average Velocity

(c) Coolant Shear Stresses
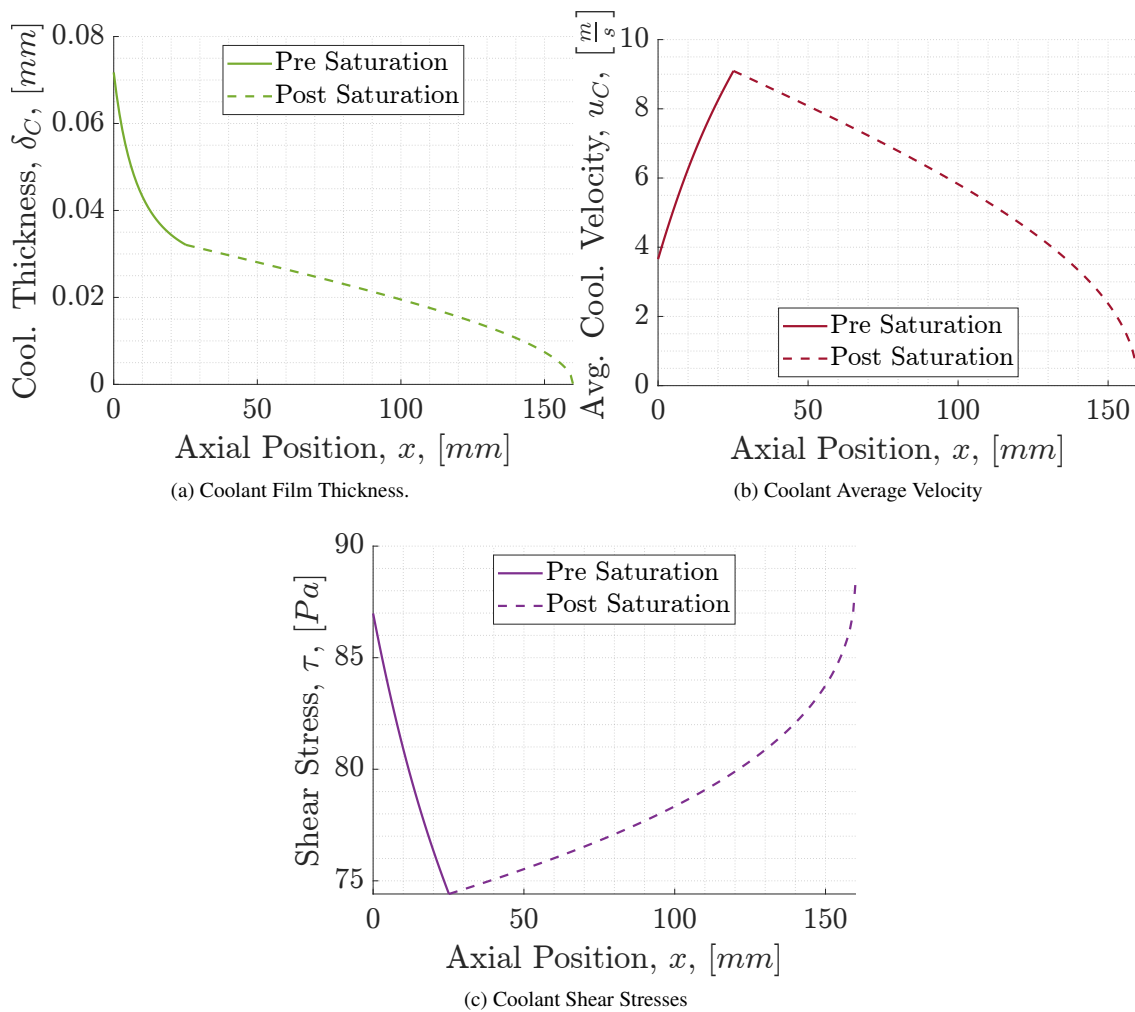
Figure 9: Momentum-Mass S1D/V1 Results, Morrel Test-8[24]

model tends to overestimate the length for which the thin layer is still liquid. Reported numerical FCLs deviate in the order of the 20 %, being in line with the averagely reported errors.[9,27] Once entrainment is activated, the numerical FCL reduces, as an effect of the enhanced convective heat transfer mechanism and the supplementary source of mass losses. As extensively reported in Sec. 4.3, for which a thorough explanation of the occurring phenomena is discussed, trying to explain the fundamental mechanism behind the new-reported behavior.

A relatively marked deviation between the model results and the experimental findings is reported. It is needed to say that the FC models are highly influenced by a specific parameter: the K_{Tu} (see Eq. 39), responsible for the enhanced convection mechanism in the presence of a turbulent motion regime. Few indications are provided for the value of this very specific parameter, whose extended expression is reported hereby:
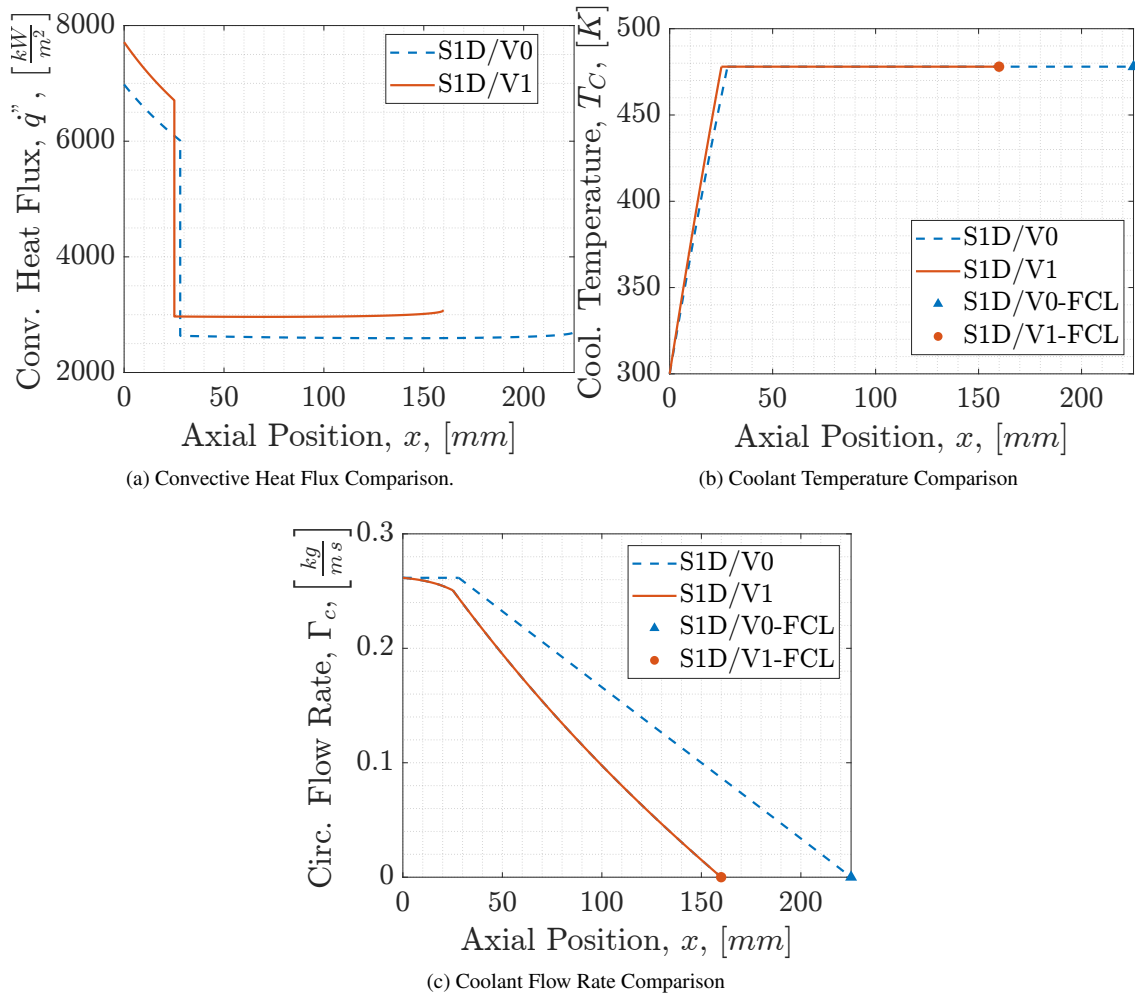
$$K_{Tu} = 1 + 4\,e_T \tag{39}$$

Where the e_T is the effective free-stream turbulence, defined as the root mean square of the turbulent velocity. Reference[9] reports values in the range 0.05-0.20, depending on the length of the considered duct.[3,11] For the present case, and for the ones in Sec. 4.5 and in Sec. 4.6 an average constant free stream turbulence intensity is considered, set to 0.10. Reference[5] provides similar results for the FCL, but without a clear statement of the turbulence values associated with every single test.

4.5 S1D Versus Kinney Data Set

In this section, the data set from Ref.[15] is exploited for the S1D model validation procedure. Considered tests and their operating conditions are reported in Tab 4. A water-film cooling investigation is carried out in 2" and 4"-diameter

LIQUID FILM COOLING ANALYSIS

(a) Convective Heat Flux Comparison.

(b) Coolant Temperature Comparison

(c) Coolant Flow Rate Comparison

Figure 10: Energy-Mass S1D Results Comparison, Morrel Test-8[24]

round tubes.

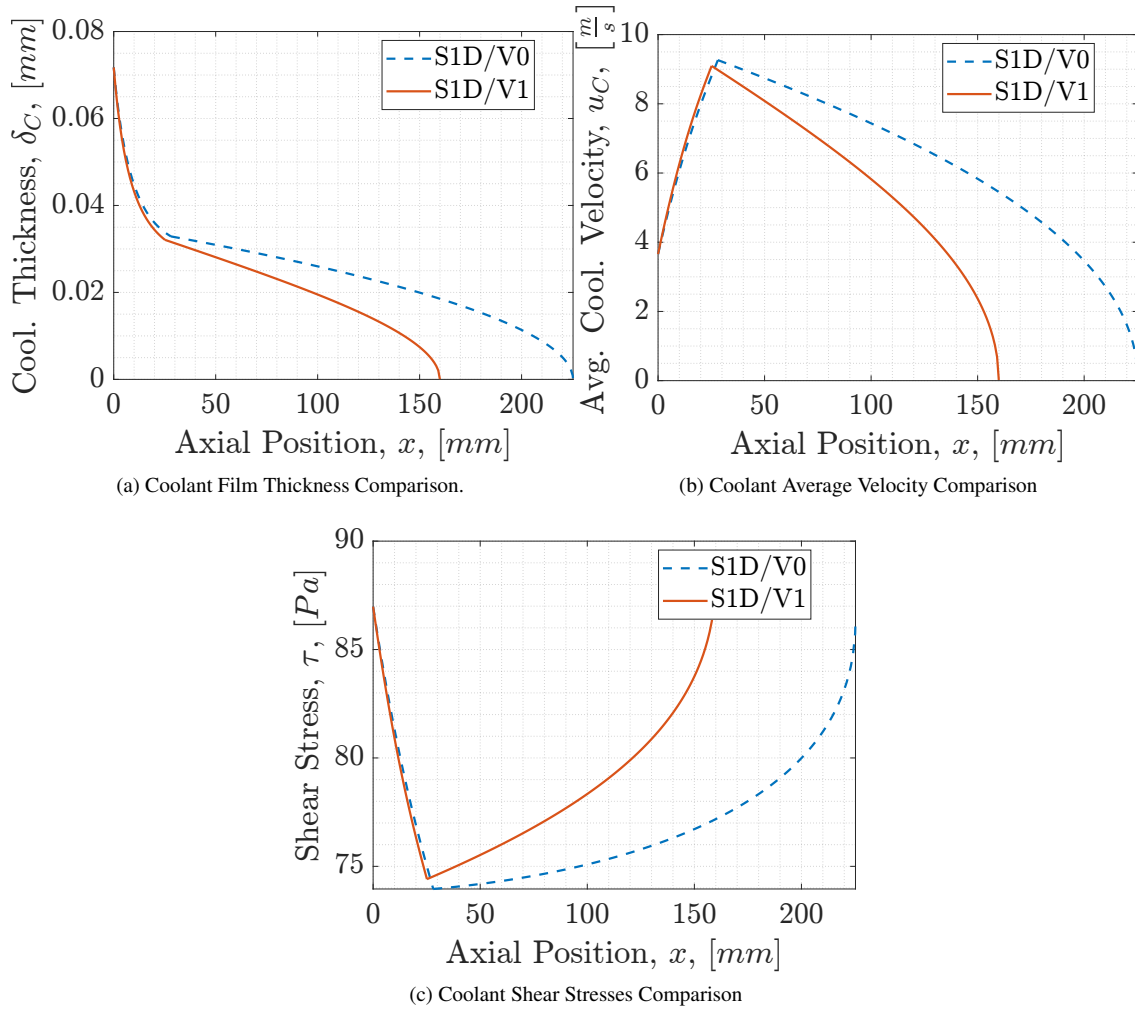| Test ID.	G_g [$kg/m^2\,s$]	Γ_c [$kg/m\,s$]	P [bar]	T [K]
KiT1	290.1	0.06	1.7	699.8
KiT2	273.9	0.10	1.7	922.0
KiT3	207.6	0.074	1.7	755.0
KiT4	222.4	0.12	1.7	1033.0

Table 4: Operating conditions for tests from Ref.[15]

In the KiT1-KiT4 data main strea fluxes vary in the range 209-290 $kg/(m^2\,s)$, and with temperature values, variables between the 700-1033 K interval. Concerning the coolant, different flow rates per unit circumference are employed and limited to the interval 0.06-0.12 $kg/(m\,s)$. The results, for the present data set, are gathered in Tab. 6.

Test ID.	Exp. *FCL* [mm]	Grissom *FCL* [mm]	Deviation [%]
KiT1	457.0	866.0	+90
KiT2	423.0	508.0	+20
KiT3	609.0	1067.0	+75
KiT4	423.0	547.0	+29

Table 5: Results from the application of Grissom's model[9] to the tests from Ref.[15]

As already witnessed for the previous data set in Sec. 3, quite different behaviors are registered whether the entrainment

(a) Coolant Film Thickness Comparison.

(b) Coolant Average Velocity Comparison

(c) Coolant Shear Stresses Comparison

Figure 11: Momentum-Mass S1D Results Comparison, Morrel Test-8[24]

is considered or not. In the absence of this phenomenon, the S1D/V0 model tends to overestimate the liquid-protected length; whereas the S1D/V1 tends to underestimate the same value. In a portion of the cases, the inclusion of entrainment reduces significantly the relative deviation, in modulus. The latter values are much more in accordance with Kinney's experimental findings, rather than the ones computed by Grissom and reported in Tab. 5.

Test ID.	Exp. *FCL* [mm]	S1D/V0 *FCL* [mm]	Deviation [%]	S1D/V1 *FCL* [mm]	Deviation [%]
KiT1	457.0	524.0	+15	312.5	-32
KiT2	423.0	545.0	+28	297.3	-30
KiT3	609.0	819.0	+34	502.2	-18
KiT4	423.0	649.0	+53	364.8	-14

Table 6: S1D model results applied to Ref.[15] data set.

Again, the final FCL results are reported to be highly dependent on the free stream turbulence intensity. As for the previous test cases, a constant 0.10 value is considered for the free stream turbulence intensity.

4.6 S1D Versus Knuth Data Set

In this last section, Knuth's data set is considered for the S1D model validation. In this framework, similar experiments to ones from Kinney are simulated. In this case, a constant-area duct with heated air is considered when water is selected as the coolant. The performed tests are labeled as KnT20, KnT45, KnT89, and KnT107, whose operating conditions are listed in Tab. 7

LIQUID FILM COOLING ANALYSIS

Test ID.	$\dot{m}_g$ [kg/s]	$\dot{m}_c$ [kg/s]]	P [bar]	T [K]
KnT20	0.770	0.028	1.1	613.0
KnT45	0.390	0.024	1.0	900.0
KnT89	0.295	0.028	1.0	1230.0
KnT107	0.699	0.068	1.1	841.0

Table 7: Operating conditions in Ref.[18]

The results for the considered tests are reported in Tab. 8 in terms of protected "numerical" length and relative deviations for both the S1D/V0 and S1D/V1 models. Differently from the other test cases, here the entrainment does not strongly vary the FCL values, except for KnT20; where a marked reduction in the percentage deviation is witnessed. In KnT45, the overestimation for S1D/V0 and the underestimation for S1D/V1 are limited to the ±3 %. Whereas for KnT89 and KnT107 the FCL is always underestimated, thus highlighting the reduced influence of the entrainment mechanism.

Test ID.	Exp. FCL [mm]	S1D/V0 FCL [mm]	Deviation [%]	S1D/V1 FCL [mm]	Deviation [%]
KnT20	1459.0	2391.0	+64	1115.7	-24
KnT45	1357.0	1400.0	+3	1399.7	-3
KnT89	1456.0	1137.0	-22	1137.1	-22
KnT107	1396.0	1138.0	-19	1138.5	-18

Table 8: S1D model results applied to Ref.[18] data set.

5. Conclusions And Future Developments

An extended open-literature review is presented, allowing for the comprehension of the physical mechanisms occurring in film cooling when applied to liquid rocket engines. The presented models foresee either the evaluation of the liquid-film-cooled length (FCL), or the wall temperature beneath the thin film. Both simplified models and more complex ones are presented. The former[6,27,29] exploits global mass and energy balances to compute the interest quantities. The latter,[9] instead, employs local balances to assess the film cooling capabilities.

Despite the simple basic physical mechanisms and the abundance of modeling techniques, the generated results lack of accuracy. This closeness gap may be deputed to all the phenomena that are not precisely described or not considered at all. One above all is the entrainment: the insurgency of roll waves over the film bore surface and the possible detachment of liquid droplets as an effect of the shearing action exerted by the main flow.

For this fact, the present article aims at filling this modeling and accuracy gap, introducing a possible characterization of this peculiar phenomenon. Hence, the hybrid rocket engine background, in liquefying fuels and relative stability, is exploited for this purpose.

Following the large literature review, a thorough description of the fundamental physical mechanism for film cooling is provided, starting from the model presented in Ref.[9] In addition to this, a precise definition of the entrainment mechanism is provided, exploiting the modeling and experimental efforts of Karabeyoglu[14] and Gater.[7] The energy, mass, and momentum balances for the thin film are defined in order to fully characterize the axial evolution of temperature, mass, velocity, thickness, and shear stresses. Therefore, a 1D space matching scheme is developed, employing the aforementioned balances, using a local description, as widely explained in Sec. 3.4 and in Sec. 3.4.

Once the model is fully developed and described, a wide validation procedure is tackled replicating the different experimental setups. The ones from Refs.[15,18,24] are exploited for validating the whole film cooling model. Moreover, the one from Gater[7] is introduced to fully corroborate the architecture for entrainment alone.

Concerning the retrieved results in Sec. 4.4, Sec. 4.5, and Sec. 4.6 better accuracy with respect to ones from Grissom are already obtained with the basic version of the code: S1D/V0. In his model, Grissom features quite large errors, up to the $\approx 80\%$, when specific data sets[15,24] are considered, and average errors $> +30\%$

When dealing with the simplified model S1D/V0, the FCL is in general overestimated (as largely witnessed in open-literature results), with errors in the $+30\%$ range, with minor outliers above this value. Once entrainment is considered, a marked reduction in the error magnitude is experienced in all the different test cases. In most of the cases, the error magnitude is in general below the 20%, when compared to the experimental results. This marks an enhanced accuracy in the modeled mechanism, considering aspects that are in general discarded, due to the complex physical relations engendering these phenomena. In general, when dealing with entrainment, the numerical FCL tends to be underestimated with respect to its experimental counterpart.

Possible future developments are surely present, specifically for the entrainment-related part. In this framework, an even finer modeling strategy may be implemented, precisely applied to the onset criteria for which this mechanism is triggered. Moreover, a more consistent description of the free-stream turbulence has to be considered, due to the strong influence of this parameter on the final FCL outcome.

References

[1] D.R. Bartz. Turbulent boundary-layer heat transfer from rapidly accelerating flow of rocket combustion gases and of heated air. volume 2 of *Advances in Heat Transfer*, pages 1–108. Elsevier, 1965.

[2] J. Bons. A Critical Assessment of Reynolds Analogy for Turbine Flows . *Journal of Heat Transfer*, 127(5):472–485, 05 2005.

[3] L.W. Carlson and W. Talmor. Gaseous film cooling at various degrees of hot-gas acceleration and turbulence levels. *International Journal of Heat and Mass Transfer*, 11(11):1695–1713, 1968.

[4] L. Crocco. An approximate theory of porous, sweat, or film cooling with reactive fluids. *Journal of the American Rocket Society*, 22:331–338, 1952.

[5] S. D Alessandro, P. Concio, M. Rotondi, D. Bianchi, and F. Nasuti. Review and implementation of engineering models of rocket film cooling and nozzle erosion. pages 1–24, 07 2022.

[6] H. W. Douglass. Liquid rocket engine self-cooled combustion chambers. Special Publication SP-8124, NASA, September 1977.

[7] R. A. Gater and M. R. L'Ecuyer. A fundamental investigation of the phenomena that characterize liquid-film cooling, 1970.

[8] R. J. Goldstein and A. Haji-Sheikh. Prediction of film cooling effectiveness. *JSME: Proceedings of 1967 semi-international symposium*, 47:213 – 218, 1967.

[9] W. M. Grissom. Liquid film cooling in rocket engines. Technical report, Morehouse College, 1991.

[10] J. E. Hatch and S. S. Papell. Use of a theoretical flow model to correlate data for film cooling or heating an adiabatic wall by tangential injection of gases of different fluid properties. Other, Technical Note NASA-TN-D-130, NASA, Lewis Research Center Cleveland, Ohio, OH, November 1959.

[11] M. Hersch. *ARS Journal*, 31, 1961.

[12] J.R. Howell, M.P. Menguc, and R. Siegel. *Thermal Radiation Heat Transfer, 5th Edition*. CRC Press, 2010.

[13] D. K. Hunzel and D. H. Hwang. Modern engineering for design of liquid rocket engines. In AIAA, editor, *Progress in Astronautics and Aeronautics*, Washington, DC, 1992. AIAA, AIAA.

[14] M. A. Karabeyoglu, D. Altman, and B. J. Cantwell. Combustion of liquefying hybrid propellants: Part 1, general theory. *Journal of Propulsion and Power*, 18:610–620, 2002.

[15] G. R. Kinney. Internal film cooling experiments with 2- and 4-inch smooth surface tubes and gas temperatures to $2000°\, f$. Technical report, NACA, 1952.

[16] C. Kirchberger, G. Schlieben, A. Hupfer, H. P. Kau, P. Martin, and S. Soller. Investigation on film cooling in a kerosene/ gox combustion chamber. 08 2009.

[17] C. U. Kirchberger. *Investigation on Heat Transfer in Small Hydrocarbon Rocket Combustion Chambers*. PhD thesis, Technische Universitat Munchen, 2014.

[18] E. L. Knuth. *The Mechanics of Film Cooling*. PhD thesis, California Institute of Technology, 1954.

[19] B. Leckner. Spectral and total emissivity of water vapor and carbon dioxide. *Combustion and Flame*, 19(1):33–48, 1972.

[20] G. Marxman and M. Gilbert. Turbulent boundary layer combustion in the hybrid rocket. *Symposium (International) on Combustion*, 9(1):371–383, 1963.

[21] G.A. Marxman, C.E. Wooldridge, and R.J. Muzzy. Fundamentals of hybrid boundary-layer combustion. In Hans G. Wolfhard, Irvin Glassman, and Leon Green, editors, *Heterogeneous Combustion*, volume 15 of *Progress in Astronautics and Rocketry*, pages 485–522. Elsevier, 1964.

[22] B.J. Mckeon, M.V. Zagarola, and A.J. Smits. A new friction factor relationship for fully developed flow. *Journal of Fluid Mechanics*, 538:429–443, 09 2005.

[23] J. Meinert, J. Huhn, E. Serbest, and O. Haidn. Turbulent boundary layers with foreign gas transpiration. *Journal of Spacecraft and Rockets*, 38:191–198, 03 2001.

[24] G. Morrel. Investigation of internal film cooling of 1000-pound-thrust liquid-ammonia - liquid oxygen rocket-engine. NACA Research Memorandum 1951-E51E05, NACA, Lewis Flight Propulsion Laboratory, Cleveland, Ohio, April 1951.

[25] R. H. Pletcher. Progress in Turbulent Forced Convection. *Journal of Heat Transfer*, 110(4b):1129–1144, 11 1988.

[26] P. Sawant, M. Ishii, and M. Mori. Droplet entrainment correlation in vertical upward co-current annular two-phase flow. *Nuclear Engineering and Design*, 238(6):1342–1352, 2008.

[27] S. R. Shine, S. Sunil Kumar, and B. N. Suresh. A new generalised model for liquid film cooling in rocket combustion chambers. *International Journal of Heat and Mass Transfer*, 55:5065–5075, 9 2012.

[28] S. R. Shine and S. Shri Nidhi. Review on film cooling of liquid rocket engines. *Propulsion and Power Research*, 7:1–18, 3 2018.

[29] R. C. Stechman, Oberstone J., and J. C. Howel. Design criteria for film cooling for small liquid-propellant rocket engines. *Journal of Spacecraft and Rockets*, 6:97–102, 1969.

[30] A.B. Metzner W.L. Friend. Turbulent heat transfer inside tubes and the analogy among heat, mass and momentum transfer. *AIChE J. 4*, 1958.